Natural Hazards
and Earth System
Sciences

Using high-resolution global climate models from the PRIMAVERA project to create a European winter windstorm event set

Julia F. Lockwood[1], **Galina S. Guentchev**[1], **Alexander Alabaster**[2], **Simon J. Brown**[1], **Erika J. Palin**[1], **Malcolm J. Roberts**[1], **and Hazel E. Thornton**[1]

[1]Met Office Hadley Centre, Exeter, EX1 3PB, UK
[2]AON, London, EC3V 4AN, UK

Correspondence: Julia F. Lockwood (julia.lockwood@metoffice.gov.uk)

Abstract. PRIMAVERA (process-based climate simulation: advances in high-resolution modelling and European climate risk assessments) was a European Union Horizon 2020 project whose primary aim was to generate advanced and well-evaluated high-resolution global climate model datasets for the benefit of governments, business and society in general. Following consultation with members of the insurance industry, we have used a PRIMAVERA multi-model ensemble to generate a European winter windstorm event set for use in insurance risk analysis, containing approximately 1300 years of windstorm data. The data are available at https://doi.org/10.5281/zenodo.6492182.

To create the storm footprints for the event set, the storms in the PRIMAVERA models are identified through tracking. A method is developed to separate the winds from storms occurring in the domain at the same time. The wind footprints are bias corrected and converted to 3 s gusts onto a uniform grid using quantile mapping. The distribution of the number of model storms per season as a function of estimated loss is consistent with re-analysis, as are the total losses per season, and the additional event set data greatly reduce uncertainty on return period magnitudes. The event set also reproduces the temporally clustered nature of European windstorms.

Since the event set is generated from global climate models, it can help to quantify the non-linear relationship between large-scale climate indices such as the North Atlantic Oscillation (NAO) and windstorm damage. Although we find only a moderate positive correlation between extended winter NAO and storm damage in northern European countries (consistent with re-analysis), there is a large change in risk of extreme seasons between negative and positive NAO states.

The intensities of the most severe storms in the event set are, however, sensitive to the gust conversion and bias correction method used, so care should be taken when interpreting the expected damages for very long return periods.

1 Introduction

Winter European windstorms are the costliest natural hazard over Europe in terms of insured losses, capable of inflicting billions of dollars of loss per event. According to Swiss Re (2018), of *all* hazards affecting Europe since 1970, the top five highest loss events (after adjusting for inflation to 2017 USD) were all winter windstorms: Daria (1990, USD 8.7 billion), Lothar (1999, USD 8.5 billion), Kyrill (2007, USD 7.2 billion), 87J (1987, USD 6.7 billion) and Vivian (1990, USD 6.5 billion).

Insurance and re-insurance companies must estimate the financial risk posed by these events to ensure they are able to pay out the resulting claims and to satisfy industry regulations. For example, European law requires that EU-based insurers hold enough capital to withstand the 1 in 200 year

loss (Solvency II, 2009), and the European Insurance and Occupational Pensions Authority (EIOPA) states that insurers must discuss the impact of climate change on their business (EIOPA, 2022), which involves assessing trends in hazards in present and future climate. A common technique used to analyse risk is catastrophe modelling, in which the insured losses due to a particular hazard are estimated by combining the hazard footprint with the clients' exposure and policy data. For European windstorms, the footprint is defined as the maximum wind gust associated with the storm over a 72 h period (Haylock, 2011), where the gust is defined as the maximum 3 s average wind speed at 10 m height, according to World Meteorological Organization observing practices (WMO, 2018). The catastrophe models can be run using either a single event footprint (e.g. a notable past event or plausible extreme future event), which can be useful for verifying the catastrophe model or understanding the vulnerability of the insurer, or an event set – a set of thousands of event footprints – to estimate large return period losses. Since observational and re-analysis datasets typically span decades rather than centuries, event set footprints must be constructed using either statistical models, dynamical (climate) models or a combination of the two.

In purely statistical methods, footprints can be generated in a variety of ways: the geospatial dependencies of observed extreme gusts can be captured in statistical models, allowing footprints to be generated from a random seed value (e.g. Youngman and Stephenson, 2016), or historical footprints can be "perturbed" to generate a number of new events that differ slightly from past ones, so are deemed to be physically plausible (e.g. Welker at al., 2021). Alternatively, a set of storm *tracks* can be generated based on the properties of historical tracks, and new footprints can be generated from the statistical relationship between tracks and footprints (e.g. Sharkey et al., 2019, 2020).

Dynamical methods using climate models are commonly used in estimations of windstorm risk, in particular with regards to estimating the effect of climate change (e.g. Leckebusch et al., 2007; Della-Marta and Pinto, 2009), but the coarse resolution of the models means that to generate an event set for use in an industry catastrophe model, statistical downscaling and bias correction of the footprints are often required. Examples include Haylock (2011), who extracted their windstorm event set from an ensemble of regional climate models at 25 km resolution, driven by coarse-resolution global climate models. The resulting footprints were downscaled further to 7 km by accounting for changes in roughness and orography between the 25 and 7 km grids. Finally, the climate model footprints were bias corrected by applying quantile mapping to historical footprints on the same 7 km grid. The Windstorm Information Service (WISC) project (Steptoe, 2017), generated an event set from the UPSCALE atmosphere-only global climate models at approximately 25 km resolution (Mizielinski et al., 2014), which were then downscaled and bias corrected to 4.4 km, again using quantile mapping to historical storms on the target grid (but without correcting for roughness and orography). Dynamical event sets can also be produced from medium to long-range ensemble prediction systems (e.g. Osinski et al., 2016; Walz and Leckebusch, 2019), in which the chaotic nature of the atmosphere means that after a few days to weeks individual storms in each ensemble member will be largely independent.

Advantages of the statistical methods include low computational costs, but they are ultimately modelled based on a short observational time period (typically less than 50 years for re-analysis and observational datasets), and although they can be used to generate thousands of footprints, the frequency of each of those footprints is difficult to estimate. The dynamical–statistical methods are computationally expensive, but the frequency of the windstorms can easily be taken directly from the model, and they are likely to be physically plausible. However, it is known that low-resolution global climate models suffer from biases in the North Atlantic storm track, where it is too zonal or displaced southwards (Zappa et al., 2013), meaning that event sets with low-resolution driving models could lead to errors in the spatial distribution of estimated storm loss.

In this paper, we describe an event set produced from the PRIMAVERA (process-based climate simulation: advances in high-resolution modelling and European climate risk assessments; https://www.primavera-h2020.eu/, last access: October 2022) high-resolution global climate model ensemble. PRIMAVERA was a European Union Horizon 2020 project whose aim was to generate advanced and well-evaluated high-resolution global climate model datasets and to interpret or process these data to meet the needs of sectors such as energy, water management, agriculture, transport, health and finance/insurance.

The event set is generated from the historical atmosphere-only experiments from five different models, at both a standard CMIP6-type resolution (typically 100 km) and at a significantly higher resolution (towards 25 km), producing approximately 1300 years of model data. Climate models run at these higher resolutions suffer less from the North Atlantic storm track biases found in models at typical CMIP5 generation and earlier resolutions ($\sim$ 200–300 km) (e.g. Zappa et al., 2013; Baker et al., 2019; Priestley et al., 2020), which should result in more realistic storm frequencies, spatial distributions and intensities. Possible reasons for this bias reduction include improvements in the representation of orographic drag which improves the simulation of climatological stationary Rossby waves (Pithan et al., 2016), increased latent heating leading to a more realistic intensification of extra-tropical cyclones (Willison et al., 2013) and a more tilted storm track (Tamarin-Brodsky and Kaspi, 2017), improvements in European blocking which help steer the storm track northwards rather than into central Europe (Schiemann et al., 2020), and sharpening of sea surface temperature (SST) gradients and reductions in SST biases leading

to changes in low-level baroclinicity and latent heat supply (Small et al., 2019).

Since the PRIMAVERA models are global, it is also possible to associate each storm with large-scale climate indices such as the North Atlantic Oscillation (NAO). Given recent advances in NAO prediction on seasonal (Scaife et al., 2014) to annual (Dunstone et al., 2016) and multi-annual (Athanasiadis et al., 2020; Smith et al., 2020) timescales, this gives insurers the possibility of using their catastrophe models in a predictive mode, assessing the change in storm risk for a given NAO forecast.

The aim of this paper is to describe the method used to create the event set from PRIMAVERA models and to show how it compares to re-analysis. The method involves first identifying the storms using a tracking algorithm, then extracting the model surface winds associated with each storm to make the footprint. The footprints from different climate models are then re-gridded to a common $0.25° \times 0.25°$ grid, and the model winds are bias corrected and converted to gusts using quantile mapping. We note that the concept of this event set is similar to the stochastic event set created for the WISC project (Steptoe, 2017). The main differences between the two event sets are (i) use of a multi-model ensemble for PRIMAVERA rather than a single model ensemble, (ii) separating the footprints of storms occurring in the same 72 h period in order to study temporal clustering and (iii) applying different bias correction methods.

The model and re-analysis data used are described in Sect. 2, and Sect. 3 gives a full description of the method. In Sect. 4 we show the comparison with re-analysis and also the relationship between storm loss and the NAO. Section 5 discusses the sensitivity of footprint intensity to the bias correction method, and conclusions are given in Sect. 6.

2 Data

2.1 PRIMAVERA model data

The event set is made from the highresSST-present PRIMAVERA experiments. These simulations are atmosphere only, covering the period 1950–2014, and use the historical forcings detailed in the HighResMIP protocol (Haarsma et al., 2016, Table 1). The lower boundary was forced by the daily, 1/4° Hadley Centre Global Sea Ice and Sea Surface Temperature (HadISST.2.2.0; Kennedy et al., 2017) dataset, with area-weighted regridding used to map this to each model grid.

The PRIMAVERA models used for the event set are summarized in Table 1. Each model was run at both a standard CMIP6-type resolution (typically 100 km) and at a significantly higher resolution (towards 25 km), and some models ran multiple ensemble members. Note that although the CMIP6-type resolution is often referred to as "low resolution", these resolutions were considered relatively high

for global models of the CMIP5 generation. For example, the CMIP5 model HadGEM2-ES on the N96 grid (∼ 135 km grid spacing at mid-latitudes) was categorized by Zappa et al. (2013) as one of the higher-resolution CMIP5 models with a small bias in the North Atlantic storm track.

A windstorm footprint is defined as the maximum *3 s gust* associated with the storm over a 72 h period, but because only two PRIMAVERA models outputted maximum gusts we instead extract daily maximum surface (10 m) winds (sfcWindmax) from the PRIMAVERA models and convert from winds to gusts as described in Sect. 3.1.3. Only data for October–March are extracted to cover the extended winter season. These winter storms tend to be associated with extra-tropical cyclones and span a larger spatial area compared to smaller, convective storms that occur in summer. The 6-hourly 850 hPa *u* and *v* winds were extracted to calculate the relative vorticity needed for the tracking algorithm to identify storms, described in Sect. 3.1.1.

2.2 Re-analysis data

To validate the PRIMAVERA event set, footprints were also made from the ECMWF Reanalysis 5th Generation (ERA5; Hersbach et al., 2020; Climate Data Store, 2022) wind gusts. This dataset covers the period 1979–2014 on a $0.25° \times 0.25°$ grid (∼ 18 km grid spacing at 50° N). Hourly maximum 3 s gusts for October–March were extracted and converted to daily maxima for fair comparison with PRIMAVERA models. A re-analysis was chosen to represent observations rather than station data because of complete spatial coverage, but we acknowledge that re-analyses can suffer from biases. There is limited literature on the validation of ERA5 gusts, although Minola et al. (2020) showed a high temporal correlation between ERA5 gusts and station observations in Sweden, with evidence of a negative bias for strong gusts over mountainous regions. We performed a comparison of the gusts in ERA5 footprints to station observations for a selection of famous historical storms revealing reasonable agreement between ERA5 and observations (see https://doi.org/10.5194/nhess-2022-12-AC1, Fig. R1).

Tracking to identify the re-analysis storms (Sect. 3.1.1) was performed on an earlier version of ECMWF re-analysis, ERA-Interim (Dee et al., 2011), since ERA5 tracks were unavailable at the time. Since Northern Hemisphere cyclone tracks have been shown to match well between re-analyses, particularly for intense cyclones (Hodges et al., 2011), the inconsistency between the tracks and gust data is expected to be small.

3 Methods

3.1 Generating the footprints

To comply with industry standards, a windstorm footprint is defined as the maximum 3 s gust associated with the

Table 1. Summary of PRIMAVERA models used for the event set. *Only two of the three ensemble members run at each resolution were used due to tracking failures.

Institution	MOHC, UREAD, NERC	EC-Earth KNMI, SHMI, BSC, CNR	CERFACS	MPI-M	CMCC
Model name	HadGEM3-GC3.1	EC-Earth3P	CNRM-CM6.1	MPI-ESM1.2	CMCC-CM2-(V)HR4
Resolution names	LM, MM, HM	LR, HR	LR, HR	HR, XR	HR4, VHR4
Model atmosphere component	MetUM	IFS cyc36r4	ARPEGE6.3	ECHAM6.3	CAM4
Atmospheric dynamical scheme (grid)	Grid point (SISL; lat–long)	Spectral (linear; reduced Gaussian)	Spectral (linear; reduced Gaussian)	Spectral (triangular; Gaussian)	Grid point (finite volume; lat–long)
Atmospheric grid name	N96; N216; N512	Tl255; Tl511	Tl127;Tl359	T127; T255	$1° \times 1°$; $0.25° \times 0.25°$
Atmospheric mesh spacing at 50° N (km)	135; 60; 25	71; 36	142; 50	67; 34	64; 18
Atmospheric nominal resolution (CMIP6)	250; 100; 50	100; 50	250; 100	100; 50	100; 25
Ensemble members at each resolution	5; 3; 3	2*; 2*	1; 1	1; 1	1; 1
Atmospheric model levels (top)	85 (85 km)	91 (0.01 hPa)	91 (78.4 km)	95 (0.01 hPa)	26 (2 hPa)
Reference(s)	Williams et al. (2018); Roberts et al. (2019)	Haarsma et al. (2020)	Voldoire et al. (2019)	Gutjahr et al. (2019)	Cherchi et al. (2019)
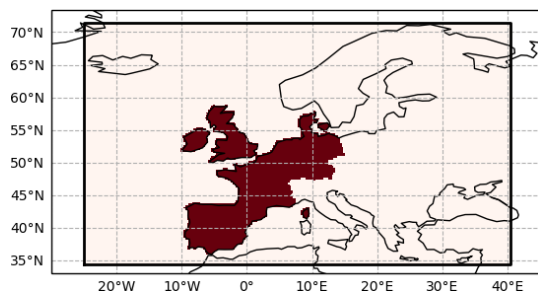
Figure 1. Footprint domain and countries used for calculation of loss index.

storm over a 72 h period. The footprint domain is defined as 25° W to 40.5° E in longitude and 34.4 to 71.5° N in latitude (Fig. 1).

Storms are first identified with the tracking algorithm (Sect. 3.1.1). One 72 h (3 d) footprint is produced per track, despite typical track lengths being longer than 72 h. Since daily data are used, each 72 h period runs from 00:00 Z on day 1 to 00:00 Z on day 4. Following Roberts et al. (2014), for each track, the central day (day 2) of the 72 h period over which to take the maximum gusts is identified by finding the day of the maximum 10 m wind speed over land within 3° of the track centre (output by the tracking algorithm).

Often two or more tracks will have the same or overlapping 72 h periods identified for their footprints. Taking the maximum winds or gusts over the whole domain for the specified 72 h period for each event would result in several cyclones being present in a single footprint, and many cyclones would be counted twice in the resulting event set. The footprints are therefore separated as described in Sect. 3.1.2. Finally, the footprints must be re-gridded to a common, high-resolution grid, converted from maximum winds to maximum 3 s gusts, and bias corrected; this is described in Sect. 3.1.3.

Footprints were made for every extra-tropical cyclone track identified by the TRACK algorithm. Many of these cyclones do not have strong enough winds to cause damage, but since users will be interested in different domains and use different estimations of storm severity or vulnerability functions, all footprints are retained so that users can perform filtering tailored to their own needs.

3.1.1 Storm tracking

The identification and tracking of the extra-tropical cyclones in the model data are performed following the approach used in Hoskins and Hodges (2002) based on the Hodges (1995, 1999) tracking algorithm (TRACK). The cyclones are tracked on the 6-hourly, T42 spectrally filtered 850 hPa relative vorticity field. Planetary waves with a wave number less than 5 are filtered out to remove the large-scale background and improve reliability of the algorithm. Only cyclones with a maximum intensity greater than 1.0×10^{-5} s^{-1} lasting at least 2 d and travelling more than 1000 km are retained for the footprints.

The tracking was performed on individual seasons (December–February, DJF, March–May, MAM, June–August, JJA, September–November, SON), but footprints were generated for all cyclones identified in the extended winter (October–March). Some cyclone tracks may have been cut short by crossing the season boundaries or split into two separate tracks, but assuming a constant cyclone formation rate throughout the season and that the severe winds of a cyclone last 72 h (as is assumed by in the insurance industry), this will only affect 3 % of tracks.

The storm tracking in the ERA-Interim re-analysis was performed in a similar way (see Roberts et al., 2014, for a full description). The main difference is that the re-analysis tracking used 3-hourly data, but only 6-hourly track positions were retained to be consistent with the PRIMAVERA model tracks.

Due to technical issues, occasionally the tracking algorithm was unable to complete a full winter season. It was not possible to diagnose the issue and re-run the tracks in the time frame available, so these seasons were removed from the event set. A total of 12 model winters were affected, listed in Appendix A.

3.1.2 Footprint separation

It was not possible to apply the method of footprint separation used in previous studies such as Roberts et al. (2014), since this was developed for 6-hourly maximum wind data rather than daily maxima. Instead, to separate footprints of storms with overlapping 72 h periods, for each day in a model run, each grid point in the daily maximum wind field is assigned to a storm track by identifying the closest cyclone track point during that day. Grid points more than 1500 km from any track point are not assigned to a cyclone track. To generate the footprint for each cyclone track, the daily maximum winds for the 72 h period (specified as above) are extracted, with the grid points assigned to other cyclones masked out, and the 72 h maximum is taken. Figure 2 demonstrates the method in ERA5 data for the observed famous storms Lothar and Martin, which struck France within 24 h of each other on 26 and 27 December 1999. Without separating the wind fields in this way, Fig. 2 shows that the footprints of Lothar and Martin would be almost identical over land.

On some occasions storm tracks can come within 1500 km of each other in the same 24 h period, making it impossible to separate the storms using daily data. In these cases the winds can be assigned to the wrong storm, and the footprints appear to have truncated wind fields (this can be seen over the Atlantic in the final footprint for storm Martin; Fig. 2h). However, inspection of footprints in the event set shows that most strong winds ($> 20\,\text{m s}^{-1}$) over land are captured in each footprint, and the truncation should not have an effect on seasonal aggregate losses.

3.1.3 Downscaling, bias correction and conversion from winds to gusts

Insurance industry windstorm footprints are typically maps of maximum 3 s gust at 10 m rather than wind speed on a very high-resolution grid (maximum grid spacing $\sim 25\,\text{km}$, although $< 10\,\text{km}$ is preferred; Bojovic et al., 2017). To be consistent with these industry standards, the footprints must be converted from wind to gust speeds and downscaled to a common grid. Here the target grid is that of the ERA5 gusts ($0.25° \times 0.25°$, approximately 18 km grid spacing at 50° N), and ERA5 gusts are taken to represent observations.

We use quantile mapping to achieve both the conversion from winds to gusts and bias correction. The method is as follows. The model daily maximum wind speeds are downscaled to the ERA5 grid using linear interpolation. At each *individual grid point*, the empirical cumulative distribution function (CDF) is calculated at probability intervals of 0.5 % up to the 98th percentile. Above the 98th percentile, the CDF is fitted using a generalized Pareto distribution (GPD), which is commonly used for fitting extreme wind speeds (e.g. Sharkey et al., 2020). Following Fawcett and Walshaw (2012), declustering to remove temporal dependence is not applied to improve precision of parameter estimates. The mean extremal index, estimated using the interval estimator of Ferro and Segers (2003), has a mean value of 0.61, so the effect of clustering on the return levels is expected to be small relative to other errors (Fawcett and Walshaw, 2012). The GPD fitting is performed separately for each model.

The quality of the GPD fits was assessed by calculating the difference between the fitted and empirical value of the 99.8th percentile. If this was found to be greater than $1\,\text{m s}^{-1}$ at a grid point i, then the parameters of the GPD fit were taken from the mean of the surrounding grid points. The CDF estimations as described above were then repeated on the ERA5 gust distribution. The model CDFs are estimated on wind speeds in the time period which overlaps with the ERA5 dataset, 1979/80–2013/14 (October–March only), to take into account any non-stationarity in the wind and gust speed distributions due to climate change and/or low frequency climate variability.

The daily maximum gust speeds, $g_i(t)$, at each grid point i and time t are then estimated using a transfer function:

$$g_i(t) = f_{\text{ERA5},i}^{-1}[f_{\text{mod},i}(w_i(t))], \tag{1}$$

where $w_i(t)$ is the daily maximum model wind speed at grid point i, and $f_{\text{ERA5},i}(x)$ and $f_{\text{mod},i}(x)$ are the estimated CDFs of the ERA5 gusts and model wind speeds at grid point i, respectively.

Quantile mapping has been used for this purpose in previous event set methodologies (e.g. Steptoe, 2017; Osinski et al., 2016), but note that here quantile mapping is performed for each grid point individually rather than pooling data over the whole domain. The reason for this is demonstrated in Fig. 3, which shows quantile–quantile (q-q) plots of the
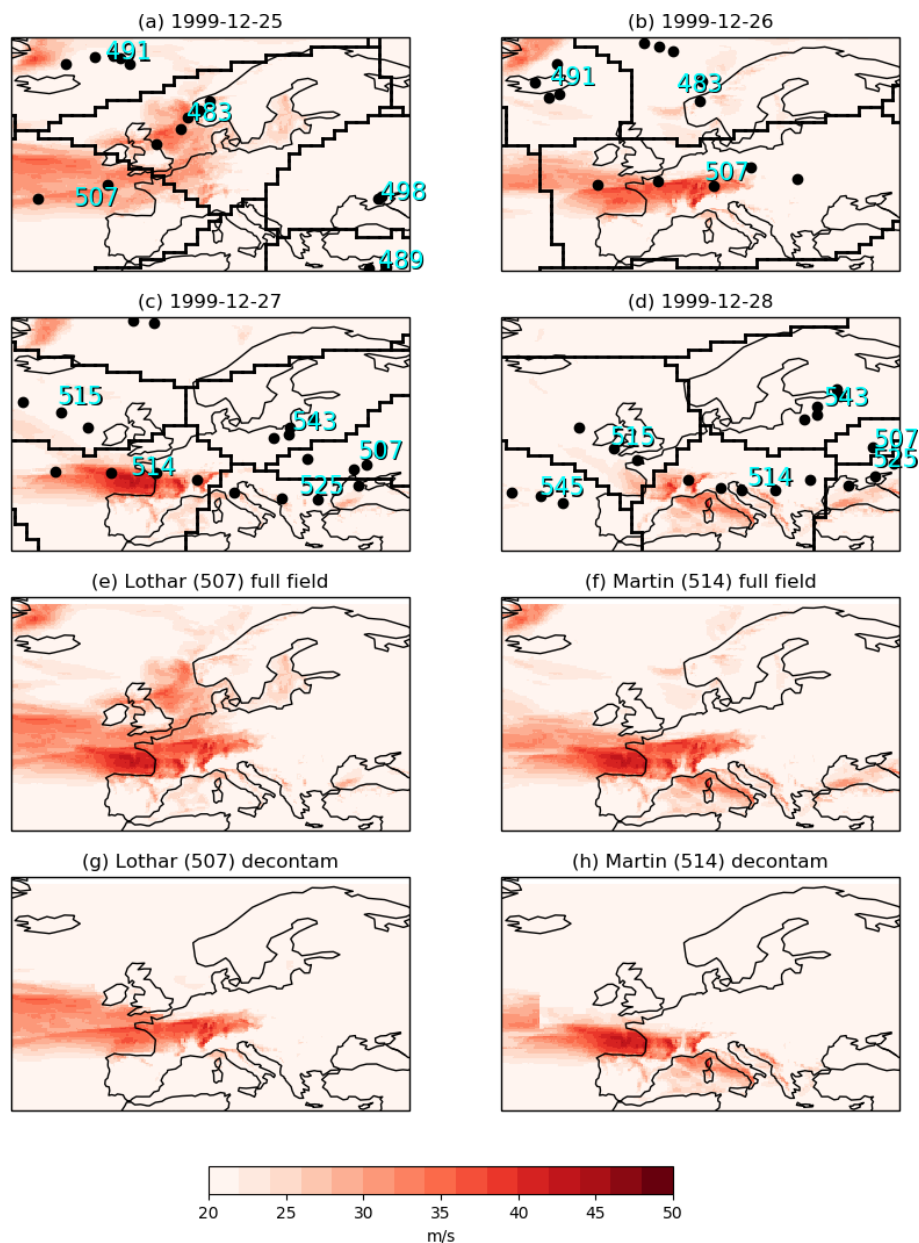
Figure 2. Storm separation method: panels **(a–d)** show the daily maximum gust fields from ERA5 for 25–28 December 1999, with the 6-hourly track points of each storm identified in the domain on that day (the cyan number gives the track identification number). The thick black lines mark the shape of the mask used for each track on each day; for example, the footprint of Lothar (track 507) is made by taking the maximum of the gusts in the marked areas around track 507 (the rest of the gusts are set to missing data) for 25–27 December. The resulting footprint is shown in panel **(g)**, compared to taking the maximum gusts over the whole domain on the same days shown in panel **(e)**. Panels **(f)** and **(h)** are the same for storm Martin (track 514).

October–March daily maximum gusts from ERA5 against the October–March daily maximum wind speeds from the PRIMAVERA model HadGEM3-GC3.1-MM (other models are shown in Appendix B) for a selection of major cities around Europe. The mapping from winds to gusts varies considerably depending on location; e.g. a $5\,\mathrm{m\,s^{-1}}$ wind speed in London maps to a gust speed of $\sim 9\,\mathrm{m\,s^{-1}}$, whereas the same wind speed in Geneva maps to a gust speed of

nearly $21\,\mathrm{m\,s^{-1}}$. One of the reasons for this discrepancy is the use of an effective roughness parametrization in climate models to take into account the effects of sub-grid-scale orography and simulate realistic orographic drag on the upper level flow (Wood and Mason, 1993; Howard and Clark, 2007; Williams et al., 2020). This can, however, lead to unrealistically low surface wind speeds, especially over high land
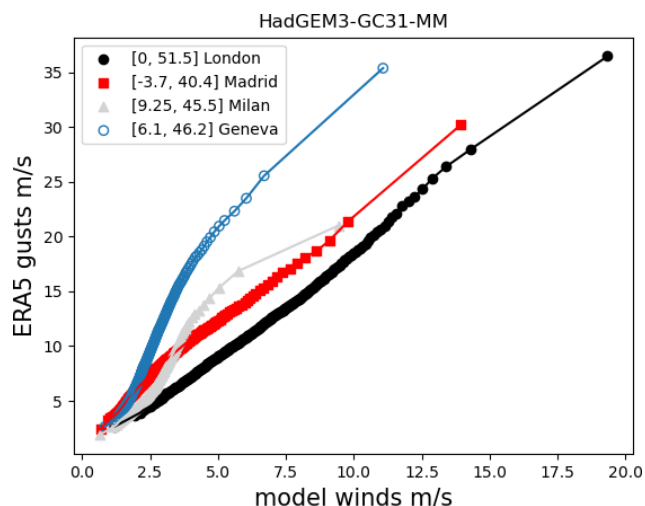
Figure 3. *q-q* plots at selected locations (points in increments of 0.5 %) showing the relationship between ERA5 daily maximum 3 s gusts and daily maximum model winds in HadGEM3-GC31-MM. The PRIMAVERA wind speeds have been linearly interpolated to the ERA5 grid.

(Roberts et al., 2014), and the degree of the bias is strongly dependent on the orographic properties of the grid point.

A disadvantage with mapping on individual grid points is that there are a limited number of data points available for fitting the GPD, so extreme gust values in the corrected footprints should be considered highly uncertain. In some cases, the mapping from model winds to gusts becomes unstable leading to unrealistically high estimated gusts, for example when an input model wind speed is greater than the maximum used in the fitting period. In these cases the estimated gusts are capped at $60 \, \mathrm{m \, s^{-1}}$ over land and $70 \, \mathrm{m \, s^{-1}}$ over sea grid points. The limitations of this method to convert wind speeds to gusts are discussed further in Sect. 5.

3.2 Loss estimation

To estimate the damage resulting from each storm in the event set, for each storm footprint we calculate a dimensionless loss index (LI), based on the index derived by Klawa and Ulbrich (2003):

$$\mathrm{LI} = \sum_i \mathrm{area}_i \times \mathrm{pop \, dens}_i \times \left(\frac{v_i}{v_{98,i}} - 1 \right)^3 \mathrm{\, for \,} v_i > v_{98,i}, \quad (2)$$

where area_i and $\mathrm{pop \, dens}_i$ are the area and population density of grid point i, v_i is the maximum gust speed in the footprint at grid point i, and $v_{98,i}$ is the 98th percentile gust speed at that same location (calculated separately for each model). Following the approach of the WISC project (Steptoe, 2017), unless stated otherwise, the area summation is over land grid points for the following countries: Luxembourg, United Kingdom, Ireland, France, Spain, Portugal, Belgium, Netherlands, Germany and Denmark (shaded coun-

tries in Fig. 1). Population data are from the Gridded Population of the World, Version 4 (GPWv4; CIESIN, 2016).

This loss index has been found to correlate well with aggregate insured losses over a season in Germany and the UK (Klawa and Ulbrich, 2003; Leckebusch et al., 2007). The index is calculated per event rather than the summation of daily data over a season, which is a commonly used modification (e.g. Karremann et al., 2014; Priestley et al., 2018). For the aggregate (total) losses per season, the LI is summed over all *events* in a season. We note that other loss indices exist (see Prahl et al., 2015, for example), and those with exponents greater than three may amplify differences between models and re-analysis compared to the results presented here.

3.3 NAO calculation

In Sect. 4.4 the NAO index is defined as the anomaly in the difference between mean sea level pressure between a region centred on the Azores (latitude 36–40° N, longitude 20–28° W) and one centred on Iceland (latitude 63–70° N, longitude 16–25° W; Dunstone et al., 2016). In this paper the extended winter mean NAO is calculated for the re-analysis and each climate model. The anomalies each winter are given with respect to the extended winter mean of the whole period available for each model (1950/51–2013/14) and the re-analysis (1979/80–2013/14), although almost identical results are obtained when anomalies are given with respect to the common period.

4 Results

4.1 Storm tracks and footprints

Footprints were generated for all extended winter tracks identified by TRACK for all models, producing a total of 1332 years of data. In total there are 268 620 footprints, 69 482 of which have a non-zero loss index (LI), and 2738 represent severe damage storms (based on the LIs of the named events in Roberts et al., 2014, these are defined as events with LI $> 1.0 \times 10^6$; such storms occur approximately once every two winters over Europe and make up 70 % of total losses). Table 2 compares the mean number of storms per extended winter in PRIMAVERA models to re-analysis for all storms, storms with a non-zero LI and severe storms. Numbers compare well with re-analysis, although all PRIMAVERA models appear to slightly underestimate the total number of storms. The number of footprints with a non-zero LI tends to increase with model resolution, possibly because to have LI > 0 there must be regions with wind speeds greater than the local 98th percentile, which may occur in a higher proportion of storms if small-scale features embedded with high wind speeds are better resolved. The mean number of severe storms per winter remains remarkably stable at approximately two storms per winter, matching the re-analysis.
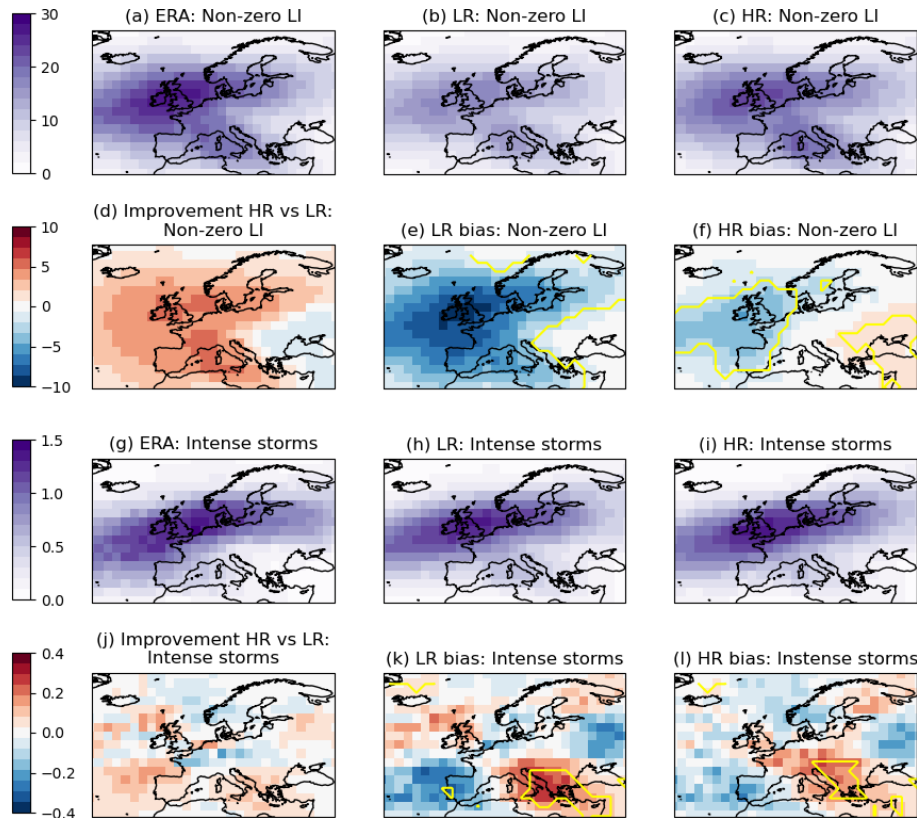
Figure 4. Track densities from re-analysis and PRIMAVERA models for tracks with a non-zero loss index (LI) and severe storms ($LI > 1 \times 10^6$). Following Economou et al. (2015), track density is defined by the number of tracks with at least one track point passing within $6.3°$ of each grid box (on a $2.5° \times 2.5°$ grid) per winter. The re-analysis track densities for non-zero LI storms are shown in **(a)** and severe storms in **(g)**. The track densities and bias (model – re-analysis) for the low-resolution PRIMAVERA models are shown in panels **(b)** and **(e)** for the non-zero LI storms (**h** and **k** for the severe storms), as well as for the higher-resolution PRIMAVERA models in panels **(c)** and **(f)** (**i** and **l** for the severe storms). The medium-resolution version of HadGEM3-GC3.1 is included in the higher-resolution models. The change in bias (| low-resolution bias | − | high-resolution bias |) from low to high resolution is shown in panel **(d)** for the non-zero LI storms and in **(j)** for the severe storms, with red areas corresponding to improvement with increased resolution. The yellow contour marks where the bias is statistically different from 0 with 95 % confidence according to Welch's unequal variances t test.

The increase in storm numbers with resolution is also reflected in Fig. 4, which shows the track densities for footprints which have non-zero LI and for severe storms only. The maximum track density is located over the UK, which is expected given the area used to calculate the LI (Fig. 1) and the fact that maximum winds tend to occur south of the tracks. The underestimation of non-zero LI tracks is most pronounced over the UK and western parts of the European continent, but the bias is much reduced in the higher-resolution models. For severe storms the bias in track density is mostly statistically insignificant over western Europe, but there is a slight over-estimation in storm numbers in the eastern Mediterranean Basin at both resolutions.

The track densities for the individual models are shown in Appendix D. The models all show the reduction in bias in non-zero LI storm numbers over western Europe as resolution increases. The response is more mixed for the intense

storms, although the biases are mostly not statistically significant.

Figure 5 shows a selection of some of the most damaging storms from the re-analysis and ones of similar strength (as measured by the LI) from the PRIMAVERA models. The figure shows that the models can simulate different "types" of storms, for example a large area storm like Daria (January 1990), intense, narrow storms such as Anatol (December 1999), storms with a southern track hitting the Iberian peninsula, such as Klaus (January 2009), and storms with a strong southwest–northeast tilt which travel northwards from Iberia to northern Europe such as 87J (the Great Storm of 1987; October 1987). Note that the model simulations are not attempting to simulate the re-analysis storms (as can be seen by the very different dates for the footprints); the figure is simply to illustrate the variety of storms that can be simulated. Also shown in Fig. 5 are the footprints for the storms with approximate return periods of 200, 100 and 50 years.

Table 2. Mean number of total footprints, footprints with a non-zero loss index and severe footprints per winter for each PRIMAVERA and re-analysis footprints. For each PRIMAVERA model, the means from both the low- and high-resolution versions are given in each row. *The model HadGEM3-GC3.1-MM is included in the "high-res" count.

Names of the low-, med- and high-resolution models	Mean number of footprints per winter			Mean number of footprints with non-zero loss index per winter			Mean number of severe footprints per winter		
	Low res	Med res	High res	Low res	Med res	High res	Low res	Med res	High res
CMCC-CM2-HR4 CMCC-CM2-VHR4	215.3		220.6	42.1		62.8	2.3		2.2
CNRM-CM6-1 CNRM-CM6-HR	198.3		216.1	44.3		61.9	2.1		2.3
EC-Earth3P EC-Earth3P-HR	200.6		199.3	52.6		66.8	2.2		2.3
HadGEM3-GC3.1-LM HadGEM3-GC3.1-MM HadGEM3-GC3.1-HM	189.9	202.6	205.96	41.6	51.5	61.7	2.0	1.8	1.8
MPI-ESM1.2-HR MPI-ESM1.2-XR	203.6		206.2	45.1		54.4	2.2		2.4
Low-res models, high-res models*	196.8	206.1		44.4	59.2		2.1	2.0	
All models		201.7			52.2			2.1	
Re-analysis		237.8			64.7			2.0	

The footprint of the 200-year event is truncated indicating it may be part of a complex cluster of storms. The 100- and 50-year events are both large-scale events over northern Europe, with footprints resembling that of Daria. There are small areas of very extreme gusts around Benelux, Germany and Poland, whose magnitude should be considered uncertain due to the bias correction (see Sect. 5).

4.2 Loss index distribution

We now examine how well the PRIMAVERA models capture the intensity distribution of storms, as measured by the loss index. Figure 6 plots the distribution of the number of severe storms (those with $LI > 1 \times 10^6$) per extended winter as a function of LI for PRIMAVERA and re-analysis data. The re-analysis dataset contains only 35 winters, so the distribution contains more noise than that for the PRIMAVERA models. For a fair comparison with the models, we therefore take 1000 random samples (with replacement) of 35 winters from the PRIMAVERA dataset to estimate the noise in a 35-winter sample. The vertical red lines on the PRIMAVERA distribution in Fig. 6 show the 95 % interval for each intensity bin based on the random samples. The re-analysis distribution lies well within the sample distributions of the models, showing that the models' and re-analysis distributions are consistent with one another.

Figure 7a shows the empirically estimated return periods for seasonal *aggregate* losses (seasonal sum of LI) in the PRIMAVERA models and the re-analysis data. The extreme tail of the PRIMAVERA data (seasons with an aggregate loss above the 90th percentile) is fitted with a GPD curve (Welker et al., 2021, Walz and Leckebusch, 2019). Note that three model storms (listed in Appendix C) had to be removed from the seasonal aggregate losses as they were considered unrealistically extreme. They are clear outliers when plotting LI against empirical return period for individual storms, and their inclusion prevented a satisfactory GPD fit. The extreme LIs are due to single grid points with extreme gusts occurring over large population centres and are a result of the bias correction method used (discussed further in Sect. 5). The aggregate losses before their removal are shown with the open red circles in Fig. 7a.

The 95 % confidence intervals on the GPD fit have been quantified by repeatedly (1000 times) randomly sampling M years of data from the fitted function (where M is the number of years of data used in the original fit, equal to 1332 for PRIMAVERA) and then re-fitting. Assuming the model LI distribution is representative of observations, the GPD fit estimates that the most extreme season over Europe in re-analysis (1989/90), which had a total LI of 4.5×10^7, has a return period of 75–200 years under present-day conditions, longer than the 35 years estimated from the re-analysis data alone.

To check if the PRIMAVERA models' return periods are consistent with the re-analysis data, as in Fig. 6, 1000 35-year samples were taken from the PRIMAVERA dataset, and
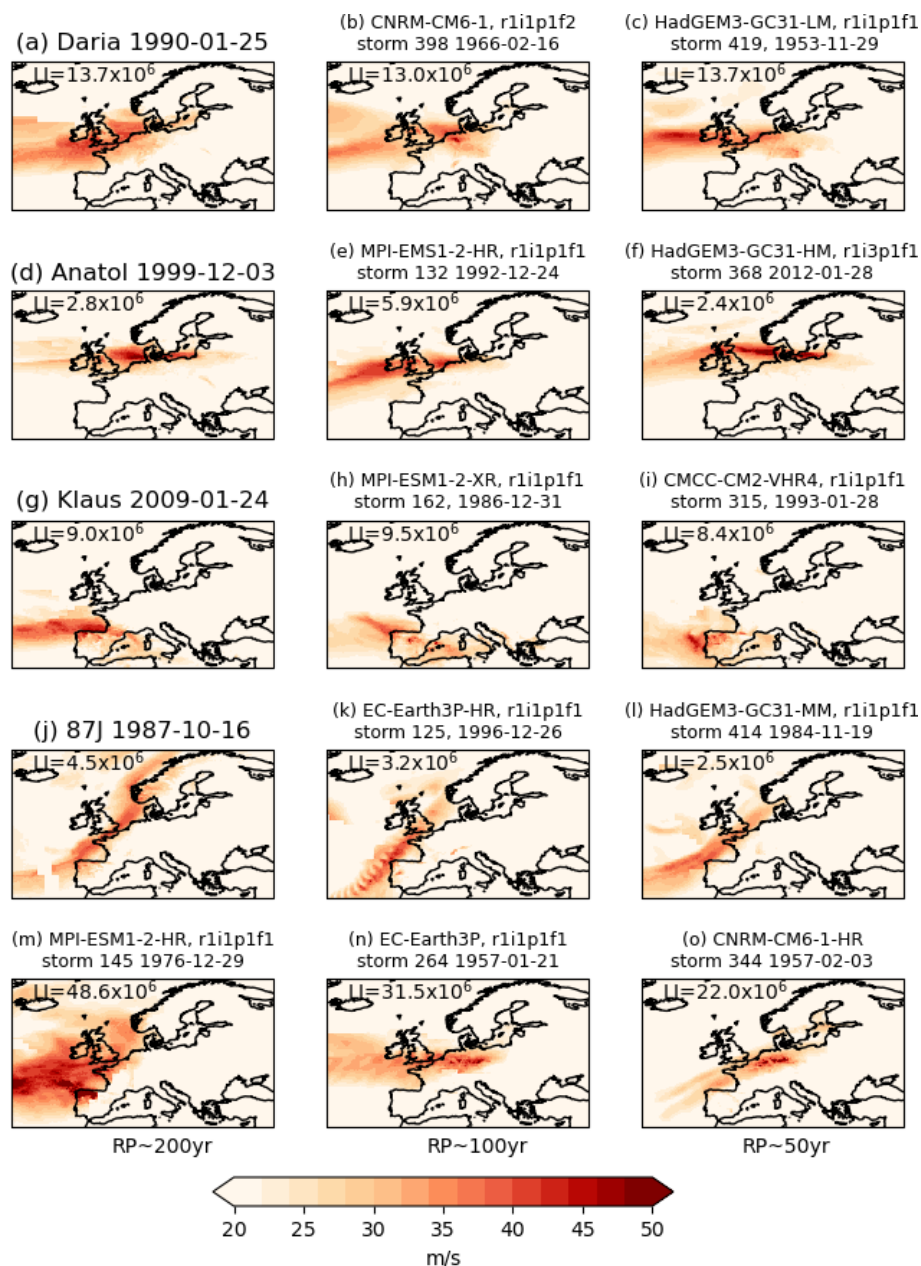
Figure 5. Example of observed and simulated footprints: left column panels (**a, d, g, j**) are re-analysis footprints of the famous storms Daria, Anatol, Klaus and 87J (the Great Storm of 1987). The footprints in the middle and right columns are from PRIMAVERA models, with each row showing two examples of storms of a similar type to the re-analysis examples. The central date of each footprint is given in the panel titles. The bottom row (**m–o**) shows the footprints for events with return periods of approximately 200, 100 and 50 years.

the 95 % intervals of the measured aggregate losses for each return period are shown with the dashed lines in Fig. 7b. The ERA5 losses are well within the bounds of the PRIMAVERA data and demonstrate the huge uncertainty in losses/return periods when only 35 years of data are used. Figure 7 also shows the return period curve for PRIMAVERA aggregate losses when an alternative bias correction and conversion to gusts is used, which is discussed further in Sect. 5.

4.3 Storm clustering

Serial (or temporal) clustering of windstorms is the tendency of these events to arrive in groups (Dacre and Pinto, 2020). It has been shown in both observations and climate models that storms are serially clustered in the flanks and exit region of the North Atlantic storm track and thus on their arrival into Europe (e.g. Mailier et al., 2006; Vitolo et al., 2009; Pinto et al., 2013; Economou et al., 2015). Priestley et al.
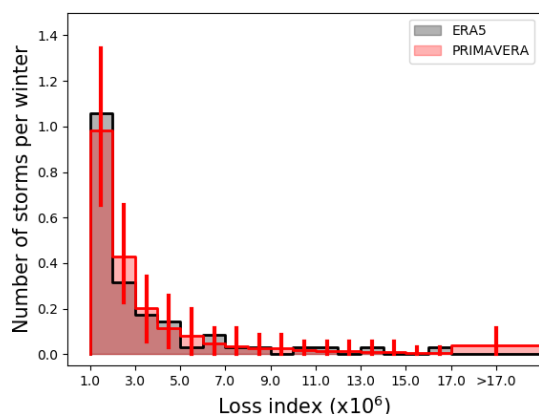
Figure 6. Distribution of the number of severe storms ($LI > 1 \times 10^6$) per extended winter as a function of LI in PRIMAVERA models (red) and re-analysis (black). Vertical red lines show the 95 % range in frequency estimated from 1000 35-year samples (with replacement) from the model data. Note that the last LI bin ($LI > 17 \times 10^6$) is larger.

(2018) demonstrated the importance of clustering in estimating losses from a high-resolution climate model, with seasonally aggregated losses 20 % higher in the (clustered) climate model output compared to random re-sampling of the data assuming a Poisson distribution for the storm frequency.

We assess clustering in the PRIMAVERA simulations by comparing the distribution of the frequency of severe storms ($LI > 1 \times 10^6$) per season to re-analysis (Fig. 8). As in Fig. 6, the consistency between PRIMAVERA and re-analysis data is assessed by taking 1000 35-year samples of PRIMAVERA data. The re-analysis distribution is consistent with being a sample from the PRIMAVERA data, and the models can even simulate seasons as extreme as winter 1989/90, with eight severe storms over Europe. There are five (of 1332) seasons in the model with eight or more severe storms, giving the chance of this occurring at least once in a 35-year period of $1 - (1327/1332)^{35} = 12$ %.

The PRIMAVERA storm numbers show a clustered distribution, with the dispersion statistic (equal to $\sigma^2/\mu - 1$, where σ^2 is the variance of storm counts per season, and μ is the mean; Mailier et al., 2006) of 0.38, which is significantly greater than zero with 95 % confidence ($p = 0.018$, estimated from the distribution of dispersion statistic assuming a Poisson distribution) and close to the re-analysis value of 0.35 (significantly greater than zero with 90 % confidence, $p = 0.07$).

4.4 Dependence on NAO

The North Atlantic Oscillation (NAO) is the primary mode of variability in the North Atlantic European region (Wallace and Gutzler, 1981) and is closely linked with the position of the North Atlantic storm track (Rogers, 1990) and consequently European windstorm damage (Walz and Leckebusch,

2019). Recent advances in the predictability of the NAO on timescales of seasons to decades (Scaife et al., 2014; Dunstone et al., 2016; Athanasiadis et al., 2020; Smith et al., 2020) have thus opened up the possibility of being able to predict European storminess on long-range timescales (Befort et al., 2019). Since the footprints in PRIMAVERA are generated from a global climate model, it is possible for insurers to extract storms associated with different NAO states to estimate the effect of the NAO on their particular portfolio and even estimate the change in expected losses for a given NAO forecast.

Figure 9a and b show the extended winter aggregate UK LIs and severe storm counts over the UK against extended winter mean NAO from PRIMAVERA models and re-analysis. The threshold for severe storms is reduced from the European LI value of 1×10^6 to 1×10^5 to take into account the smaller area and population of the UK. The UK is chosen as an example because it is well within the northern region of influence of the NAO (e.g. Hurrell and Deser, 2009).

Figure 9a shows there is a non-linear relationship between aggregate storm loss and NAO, with a clear increase in risk of a high-loss season as NAO increases. Although the rank correlation coefficients (ρ) between aggregate losses and NAO for PRIMAVERA and re-analysis are modest (0.29 and 0.41, respectively, both statistically significantly different from zero with > 95 % confidence), PRIMAVERA data estimate that the probability of an extreme season over the UK (defined as having an aggregate seasonal loss above the 90th percentile, 4×10^6) increases to 0.2 for NAO > 5 hPa and decreases to just 0.06 for NAO < -5 hPa.

There is a similar positive correlation for the *number* of severe storms striking the UK each winter ($\rho = 0.32$ for PRIMAVERA and 0.40 for re-analysis; see Fig. 9b). Figure 9c shows the correlations between extended winter NAO and aggregate losses for the other countries in the domain and shows the expected relationship with positive (negative) correlations for the northern (southern) countries. The 95 % significance levels for the PRIMAVERA data (from a two-tailed t test) are shown by the dashed red lines, indicating that all the PRIMAVERA correlations (shown by the red dots) are statistically significant. As before, consistency with ERA5 is tested by randomly sampling 35-year time series from the PRIMAVERA dataset, and the 95 % range of correlations for 35-year samples are shown by the vertical solid red lines in Fig. 9c. All the ERA5 correlations are within the bounds of the PRIMAVERA data.

5 Uncertainty in storm severity due to the bias correction and conversion to gusts method

Figure 7 showed that there were three model storms with unrealistically high loss indices, which had to be removed from the seasonal aggregate losses to obtain a satisfactory
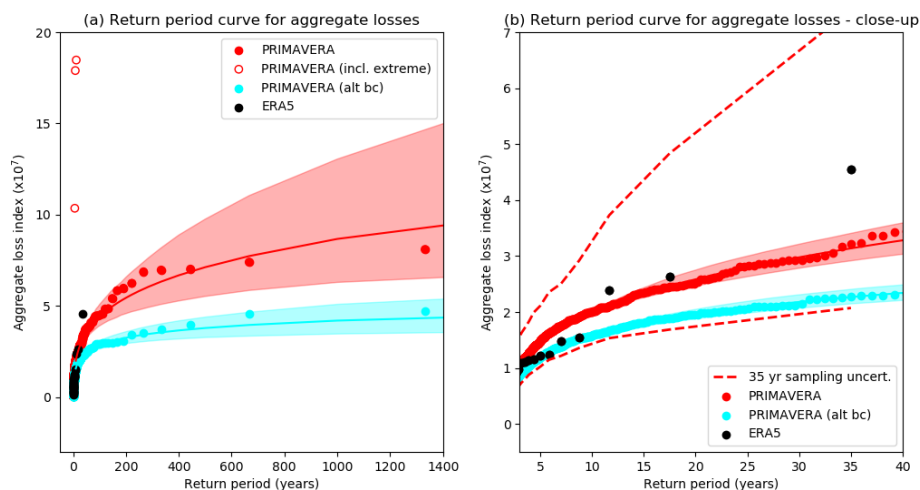
Figure 7. Return period curve for seasonal aggregate losses. The GPD fit to PRIMAVERA data is shown by the red line, with individual seasons shown by the red dots. The open red circles show the aggregate losses for the three seasons which contained the unrealistically extreme storms before these storms were removed from the aggregate (plotted at the same return period). The cyan points show the losses from the PRIMAVERA data using an alternative bias correction and gust conversion method described in Sect. 5. The shading shows the 95 % confidence intervals to the GPD fits, estimated by re-sampling. ERA5 data are shown in black. Panel **(b)** is a close-up version of panel **(a)**. The dashed lines in **(b)** show the 95 % confidence intervals in LI for a given return period when sampling 35 years of PRIMAVERA data.
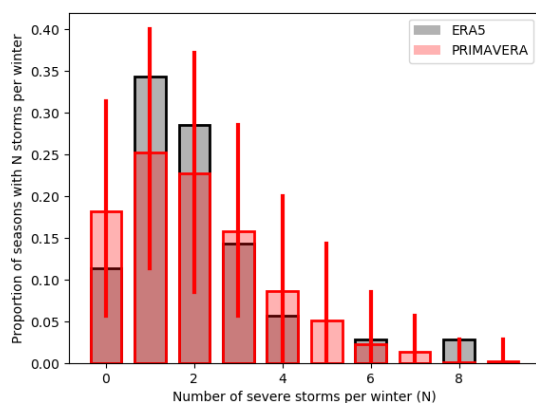
Figure 8. Distribution of number of severe storms per winter in PRIMAVERA models (red) and re-analysis (black). The red lines on each bar show the 95 % range of season counts for 1000 35-year re-samples of PRIMAVERA data.

GPD fit for the calculation of return periods. This is due to the quantile mapping method to bias correct and convert to gusts, which relied on GPD fits of the daily PRIMAVERA model and ERA5 winds/gusts (Sect. 3.1.3). As the GPD fitting is performed separately for each model over the common time period with ERA5 and at individual grid points, only 35 years of data are available for each fit (apart from where multiple ensemble members are available). Inspection of the most extreme footprint shows an intense storm centred over Barcelona, where the input raw model winds in this region were substantially greater than the maximum model winds used in the GPD fitting period. Due to the high sensitivity of

the transfer functions and the fact that the loss index is population weighted and dependent on the cube of the gust, the high gusts in this area have a huge impact on the resulting loss index.

In fact, all of the 10 most intense model storms (as measured by the LI) were for storms outside the fitting period used for the bias correction, indicating large uncertainty in the maximum gusts possible at each grid point. In addition, 9 of the 10 most intense model storms are centred on southern Europe, off the main storm track, where excessive gusts will have a larger impact on the LI due to the lower 98th local gust percentile. A total of 9 of the 10 most intense storms are also produced from the lower-resolution version of each model, which may indicate issues in the transfer functions when there is a large change in resolution from native to target grid.

Therefore, to estimate the sensitivity of LI to the estimated cumulative distribution function of ERA5 gusts and model winds, we tested using an empirical quantile mapping method (e.g. Steptoe, 2017; Osinski et al., 2016) to convert from winds to gusts. Here, instead of fitting the CDF of the gusts and winds with a GPD curve, we linearly interpolate between the empirically estimated quantiles. When an input model wind is greater than the maximum wind used in the fitting period, it is converted to the maximum ERA5 gust in the fitting period at that grid point.

Figure 10 shows a scatter plot of the loss index of each storm with this alternative bias correction method against the original loss index. There is strong agreement between the two methods, although the original method tends to give
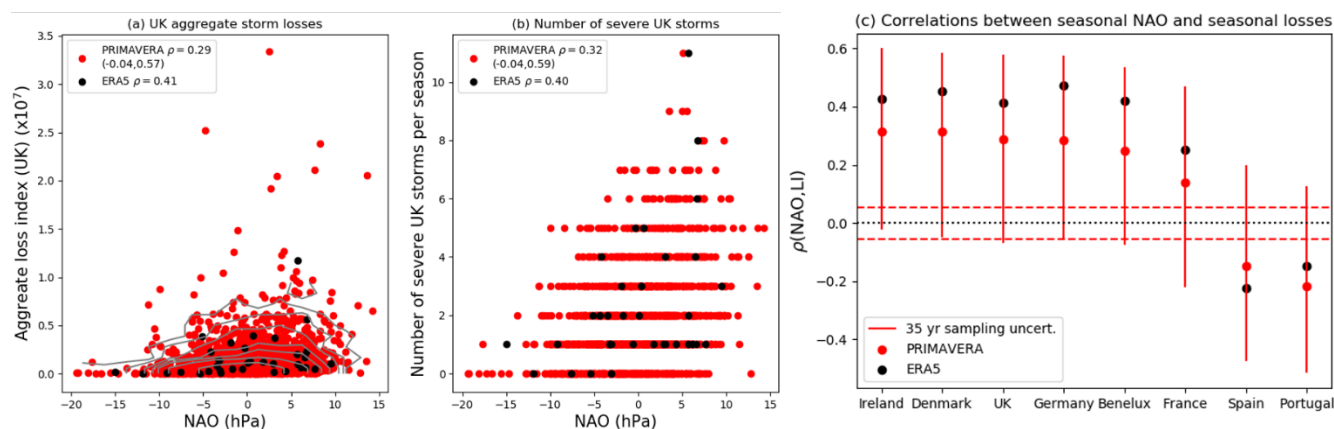
Figure 9. The relationship between extended winter NAO and storm damage. **(a)** Scatter plot of extended winter aggregate loss over the UK against extended winter NAO for PRIMAVERA and re-analysis data. Contour levels (for aggregate losses $< 1 \times 10^7$) are shown to illustrate the density of PRIMAVERA data. The contour levels are 2, 5, 10, 20, 30, 50 and 100 seasons, in bins of 2.5 hPa width in NAO and 1.1×10^6 in aggregate losses. The rank correlation coefficients between aggregate losses and NAO are given in the legend. For PRIMAVERA data, the 95 % range of correlation coefficients when taking 1000 35-year random samples random samples is also shown in brackets. **(b)** As in **(a)** but showing the number of severe UK storms (UK LI $> 1 \times 10^5$) per season. **(c)** Rank correlation coefficients between seasonal aggregate LI and NAO over the countries in the European domain for PRIMAVERA (red dots) and re-analysis (black dots). The vertical solid red lines indicate the 95 % distribution of correlations from 1000 35-year samples from PRIMAVERA data (not the confidence intervals on the correlation coefficient of all 1332 years of data), to show consistency with re-analysis. The dashed red lines show the 95 % confidence intervals of correlation coefficients for 1332 years of uncorrelated data: PRIMAVERA correlations are all outside these intervals indicating a significant difference from zero correlation with at least 95 % confidence.
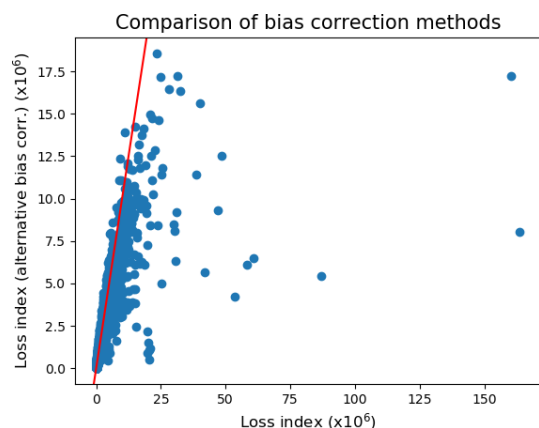

Figure 10. Scatter plot of European LI for individual footprints from the alternative bias correction method (Sect. 5) against LI using the original method. The red line shows equality.

higher intensities. A few (~ 20) storms show a large discrepancy, with substantially higher LIs using the original bias correction method. The estimations of LI for these storms (when calculated over the countries shown in Fig. 1) should be considered unreliable.

Figure 7 shows the return period curve for the aggregate losses with the alternative bias correction method (plotted in cyan). Figure 7b shows that this curve starts to diverge from the original dataset around the 5-year return period. It is likely that the alternative bias correction method gives an un-

derestimation of the "true" losses, since maximum gusts cannot be greater than those in ERA5. Nevertheless, it demonstrates the sensitivity of loss estimations for long return periods to the bias correction method used. It also shows that the uncertainty in the GPD fit to the model data does not cover the uncertainty arising from the LI values themselves.

Other bias correction methods include correcting for the effective roughness parametrization, which leads to the underestimation of model winds, as described in Howard and Clark (2007) (or a simplified version in Haylock, 2011), or pooling data for the GPD fits and allowing for dependencies on covariates such as altitude, roughness and latitude (see, for example, Economou et al., 2014, who pooled mean sea level pressure data from North Atlantic storm tracks to fit GPD functions but included dependence on latitude and NAO in the fit parameters). Alternatively, the relationship between winds on the native grid and high-resolution gusts can be modelled (for example using linear regression) if there are like-for-like footprints on both grids. This was not possible here since PRIMAVERA models are free-running and not attempting to simulate individual storms in ERA5, but this could be achieved by dynamically downscaling a selection of model footprints, as in Haas and Pinto (2012).

6 Conclusions

We have produced a freely available winter windstorm event set from PRIMAVERA global climate models for use in insurance risk analysis, which consists of 268 620 windstorm footprints, covering 1332 years of data. The data are freely available at https://doi.org/10.5281/zenodo.6492182. The method developed to create the event set separates the footprints of storms in the domain during overlapping time periods, allowing characteristics such as storm clustering to be studied more easily. To be consistent with the insurance industry definition of a footprint, the raw model winds were statistically converted to gusts on a $0.25° \times 0.25°$ grid. The intensities of the most severe storms in the event set are, however, sensitive to the gust conversion and bias correction method used.

The damage over Europe from each storm is estimated with a loss index. The frequency distribution of estimated European windstorm losses from the resulting event set, as well as the total losses per season, is consistent with re-analysis, and the additional event set data greatly reduce uncertainty on return period magnitudes. The event set also reproduces the distribution of the number of severe European storms per season seen in re-analysis, which is statistically distinct from a Poisson distribution and confirms the temporally clustered nature of severe European windstorms. The PRIMAVERA data suggest that the total loss of the most extreme season in the re-analysis data, winter 1989/90, has a return period of 75–200 years (in present-day conditions), longer than the empirical estimation from re-analysis (35 years).

The model also simulates a relationship between extended winter aggregate storm loss and the extended winter mean NAO, consistent with the re-analysis data. Although only moderate (but statistically significant) positive correlations between seasonal NAO and aggregate losses are found for northern European countries, the probability of extreme losses in a season (> 90th percentile) for the UK increase by a factor of 4 in positive NAO (NAO > 5 hPa) seasons compared to negative ones (NAO < −5 hPa). Since monthly NAO values are provided with the dataset, this allows users to investigate the effect of NAO on their individual portfolios, and to quantify the impact of a given NAO forecast, opening the possibility of predictive catastrophe modelling. The data presented in this paper are for the multi-model ensemble, but similar conclusions are reached when looking at individual models.

Future work includes refining the conversion to gusts and bias correction method and extending the event set to include the coupled PRIMAVERA simulations, as well as the PRIMAVERA climate projections which run to 2050.

Appendix A

The following model winters were removed from the event set due to incomplete tracking:

- CMCC-CM2-VHR4_highresSST-present_r1i1p1f1: 1993/1994

- EC-Earth3P-HR_highresSST-present_r3i1p1f1: 1982/3 1983/4 1966/67 1967/68

- EC-Earth3P_highresSST-present_r1i1p1f1:   1950/51 1951/52

- EC-Earth3P_highresSST-present_r3i1p1f1:   1962/63 1963/64 1970/71 1971/72

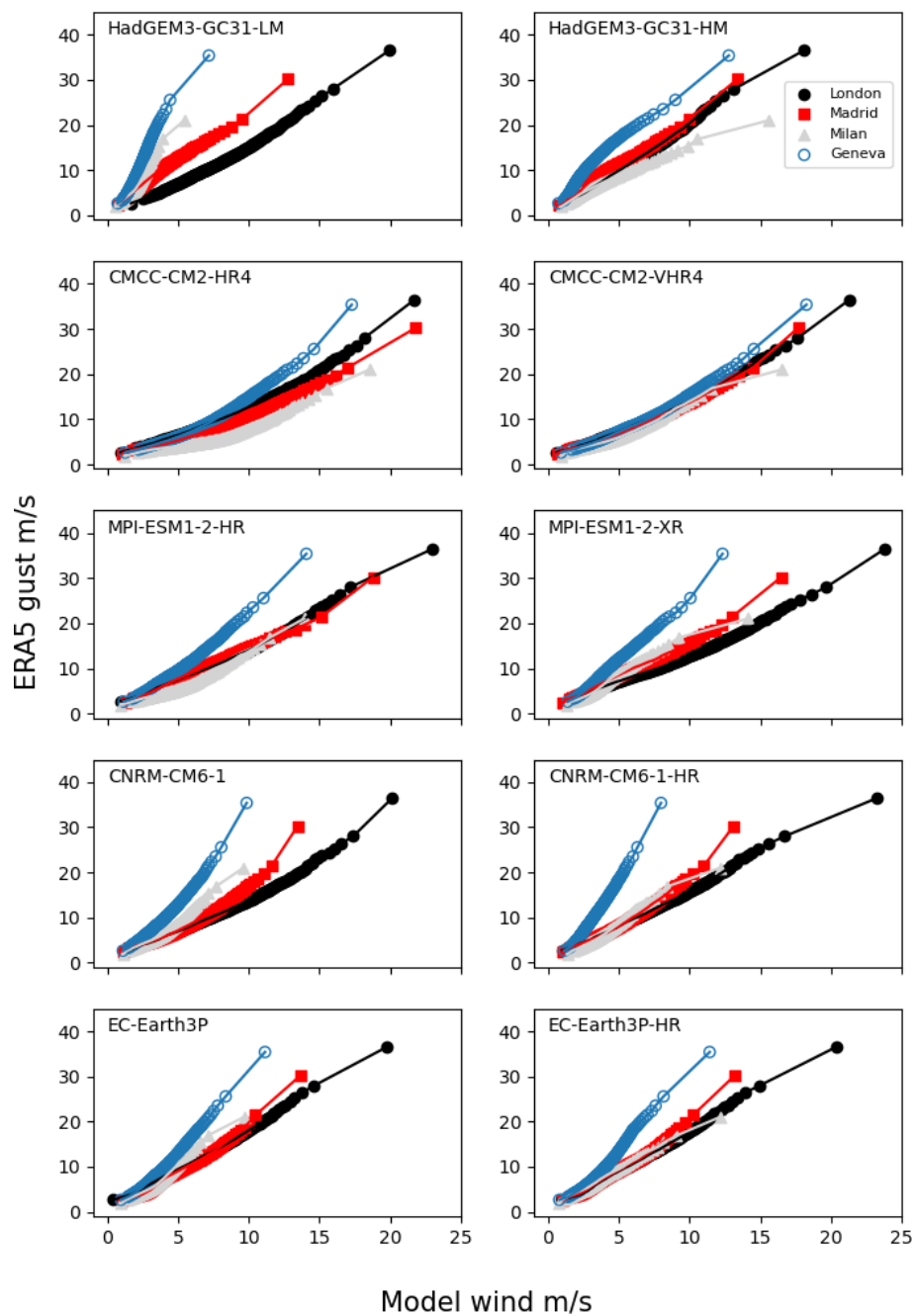- HadGEM3-GC31-HM_highresSST-present_r1i3p1f1: 2006/7

Appendix B

Figure B1. As in Fig. 3 but for the remaining PRIMAVERA models.

Appendix C

List of the 10 most extreme footprints in the event set according to European loss index. The first three storms were excluded from the seasonal aggregate losses when fitting the return period curve in Fig. 7.

– CMCC-CM2-HR4_highresSST-present_r1i1p1f1_winter1957-1958_MAM_storm123_1958-03-24_regrid_corrected.nc, $LI = 163.7 \times 10^6$

– EC-Earth3P_highresSST-present_r3i1p1f1_winter1954-1955_DJF_storm294_1955-01-29_regrid_corrected.nc, $LI = 160.3 \times 10^6$

– CNRM-CM6-1-HR_highresSST-present_r1i1p1f2_winter1974-1975_SON_storm267_1974-11-05_regrid_corrected.nc, $LI = 86.9 \times 10^6$

– HadGEM3-GC31-LM_highresSST-present_r1i2p1f1_winter1963-1964_SON_storm265_1963-10-25_regrid_corrected.nc, $LI = 60.9 \times 10^6$

– CMCC-CM2-HR4_highresSST-present_r1i1p1f1_winter1978-1979_DJF_storm29_1978-12-06_regrid_corrected.nc, $LI = 58.2 \times 10^6$

– CMCC-CM2-HR4_highresSST-present_r1i1p1f1_winter1968-1969_MAM_storm2_1969-03-13_regrid_corrected.nc, $LI = 53.5 \times 10^6$

– MPI-ESM1-2-HR_highresSST-present_r1i1p1f1_winter1976-1977_DJF_storm145_1976-12-29_regrid_corrected.nc, $LI = 48.6 \times 10^6$

– HadGEM3-GC31-LM_highresSST-present_r1i14p1f1_winter1963-1964_DJF_storm240_1964-01-10_regrid_corrected.nc, $LI = 46.9 \times 10^6$

– CMCC-CM2-HR4_highresSST-present_r1i1p1f1_winter1960-1961_MAM_storm12_1961-03-05_regrid_corrected.nc, $LI = 41.8 \times 10^6$

– HadGEM3-GC31-LM_highresSST-present_r1i1p1f1_winter1958-1959_DJF_storm303_1959-01-25_regrid_corrected.nc, $LI = 40.3 \times 10^6$
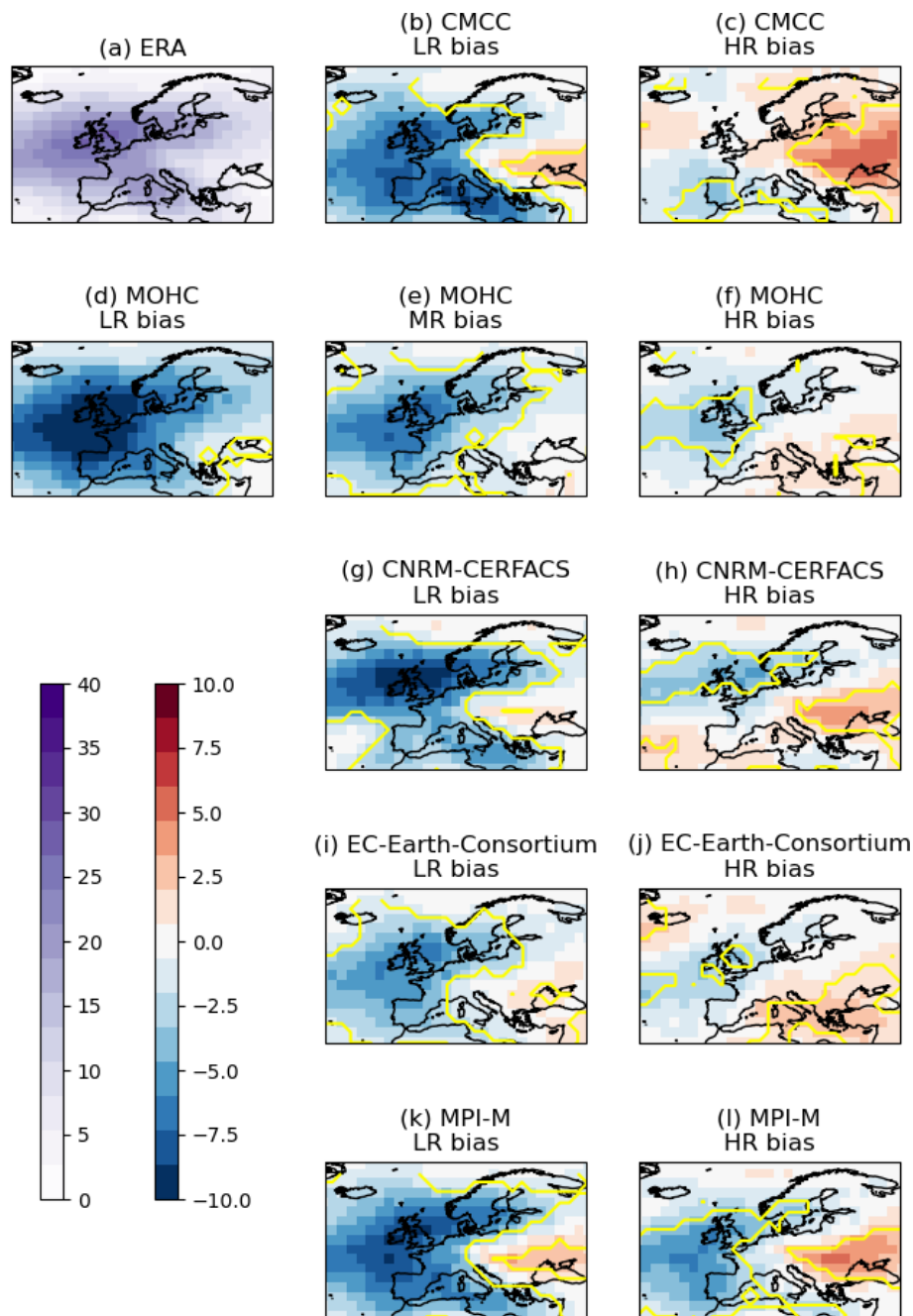
Appendix D

Figure D1. Track density bias (model − ERA) for storms with a non-zero loss index over Europe for individual models for the period October–March 1979/80–2013/14. The yellow contour marks where the bias is statistically different from 0 with 95 % confidence according to Welch's unequal variances *t* test.
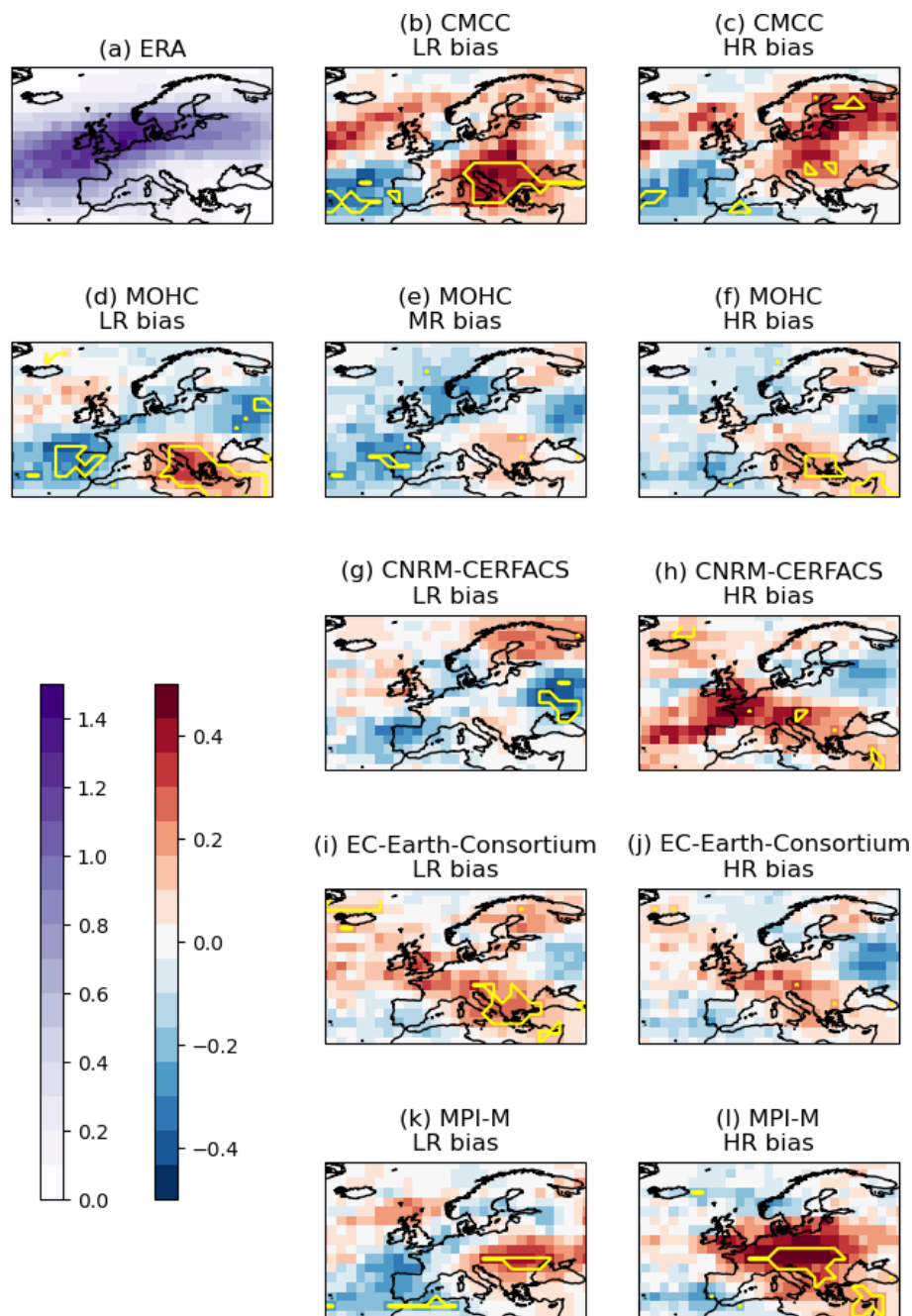
Figure D2. As for Fig. D1 but for severe storms only ($LI > 1 \times 10^6$).

References

Athanasiadis, P. J., Yeager, S., Kwon, Y.-O., Bellucci, A., Smith, D., and Tibaldi, S.: Decadal predictability of North Atlantic blocking and the NAO, npj Clim. Atmos. Sci., 3, 20, https://doi.org/10.1038/s41612-020-0120-6, 2020.

Baker, A. J., Schiemann, R., Hodges, K. I., Demory, M., Mizielinski, M. S., Roberts, M. J., Shaffrey, L. C., Strachan, J., and Vidale, P. L.: Enhanced Climate Change Response of Wintertime North Atlantic Circulation, Cyclonic Activity, and Precipitation in a 25-km-Resolution Global Atmospheric Model, J. Climate, 32, 7763–7781, https://doi.org/10.1175/JCLI-D-19-0054.1, 2019.

Befort, D. J., Wild, S., Knight, J. R., Lockwood, J. F., Thornton, H. E., Hermanson, L., Bett, P. E., Weisheimer, A., and Leckebusch, G. C.: Seasonal forecast skill for extratropical cyclones and windstorms, Q. J. Roy. Meteorol. Soc., 145, 92–104, https://doi.org/10.1002/qj.3406, 2019.

Bojovic, D., Mishra, N., Palin, E., Guentchev, G., Lockwood, J., Brayshaw, D., Gonzalez, P., Bessembinder, J., and van der Linden, E.: PRIMAVERA Deliverable D11.6: Report on end-user requirements, https://www.primavera-h2020.eu/assets/media/uploads/d11.6_v1.0_end_user_reqts.pdf (last access: November 2022), 2017.

Center for International Earth Science Information Network – CIESIN – Columbia University: Gridded Population of the World, Version 4 (GPWv4): Population Density, NASA Socioeconomic Data and Applications Center (SEDAC), Palisades, NY, https://doi.org/10.7927/H4NP22DQ (last access: July 2017), 2016.

Cherchi, A., Fogli, P. G., Lovato, T., Peano, D., Iovino, D., Gualdi, S., Masina, S., Scoccimarro, E., Materia, S., Bellucci, A., and Navarra, A.: Global mean climate and main patterns of variability in the CMCC-CM2 coupled model, J. Adv. Model. Earth Sy., 11, 185–209, https://doi.org/10.1029/2018MS001369, 2019.

Climate Data Store: Climate data repository, https://cds.climate.copernicus.eu/#!/home, last access: February 2022.

Dacre, H. F. and Pinto, J. G.: Serial clustering of extratropical cyclones: a review of where, when and why it occurs, npj Clim. Atmos. Sci., 3, 48, https://doi.org/10.1038/s41612-020-00152-9, 2020.

Dee, D. P., Uppala, S. M., Simmons, A. J., Berrisford, P., Poli, P., Kobayashi, S., Andrae, U., Balmaseda, M. A., Balsamo, G., Bauer, P., Bechtold, P., Beljaars, A. C. M., van de Berg, L., Bidlot, J., Bormann, N., Delsol, C., Dragani, R., Fuentes, M., Geer, A. J., Haimberger, L., Healy, S. B., Hersbach, H., Hólm, E. V., Isaksen, L., Kållberg, P., Köhler, M., Matricardi, M., McNally, A. P., Monge-Sanz, B. M., Morcrette, J.-J., Park, B.-K., Peubey, C., de Rosnay, P., Tavolato, C., Thépaut, J.-N., and Vitart, F.: The ERA-Interim reanalysis: configuration and performance of the data assimilation system, Q. J. Roy. Meteor. Soc., 137, 553–597, https://doi.org/10.1002/qj.828, 2011.

Della-Marta, P. M. and Pinto, J. G.: Statistical uncertainty of changes in winter storms over the North Atlantic and Europe in an ensemble of transient climate simulations, Geophys. Res. Lett., 36, L14703, https://doi.org/10.1029/2009GL038557, 2009.

Dunstone, N., Smith, D., Scaife, A., Hermanson, L., Eade, R., Robinson, N., Andrews, M., and Knight, J.: Skilful predictions of the winter North Atlantic Oscillation one year ahead, Nat. Geosci., 9, 809–814, https://doi.org/10.1038/ngeo2824, 2016.

Earth System Grid Federation: ESGF Portal at CEDA, https://esgf-index1.ceda.ac.uk/projects/esgf-ceda/, last access: November 2022.

Economou, T., Stephenson, D., and Ferro, C.: Spatio-temporal modelling of extreme storms, Ann. Appl. Stat., 8, 2223–2246,, 2014.

Economou, T., Stephenson, D. B., Pinto, J. G., Shaffrey, L. C., and Zappa, G.: Serial clustering of extratropical cyclones in a multi-model ensemble of historical and future simulations. Q. J. Roy. Meteor. Soc., 141, 3076–3087, https://doi.org/10.1002/qj.2591, 2015.

EIOPA: Consultation on Application guidance on running climate change materiality assessment and using climate change scenarios in the ORSA, Technical Report, https://www.eiopa.europa.eu/document-library/consultation/consultation-application-guidance-running-climate-change-materiality-0, last access: June 2022.

Fawcett, L. and Walshaw, D.: Estimating return levels from serially dependent extremes, Environmetrics, 23, 272–283, https://doi.org/10.1002/env.2133, 2012.

Ferro, C. A. T. and Segers, J.: Inference for clusters of extreme values, J. R. Stat. Soc. B, 65, 545–556, https://doi.org/10.1111/1467-9868.00401, 2003.

Gutjahr, O., Putrasahan, D., Lohmann, K., Jungclaus, J. H., von Storch, J.-S., Brüggemann, N., Haak, H., and Stössel, A.: Max Planck Institute Earth System Model (MPI-ESM1.2) for the High-Resolution Model Intercomparison Project (HighResMIP), Geosci. Model Dev., 12, 3241–3281, https://doi.org/10.5194/gmd-12-3241-2019, 2019.

Haarsma, R., Acosta, M., Bakhshi, R., Bretonnière, P.-A., Caron, L.-P., Castrillo, M., Corti, S., Davini, P., Exarchou, E., Fabiano, F., Fladrich, U., Fuentes Franco, R., García-Serrano, J., von Hardenberg, J., Koenigk, T., Levine, X., Meccia, V. L., van Noije, T., van den Oord, G., Palmeiro, F. M., Rodrigo, M., Ruprich-Robert, Y., Le Sager, P., Tourigny, E., Wang, S., van Weele, M., and Wyser, K.: HighResMIP versions of EC-Earth: EC-Earth3P and EC-Earth3P-HR – description, model computational performance and basic validation, Geosci. Model Dev., 13, 3507–3527, https://doi.org/10.5194/gmd-13-3507-2020, 2020.

Haarsma, R. J., Roberts, M. J., Vidale, P. L., Senior, C. A., Bellucci, A., Bao, Q., Chang, P., Corti, S., Fučkar, N. S., Guemas, V., von Hardenberg, J., Hazeleger, W., Kodama, C., Koenigk, T., Leung, L. R., Lu, J., Luo, J.-J., Mao, J., Mizielinski, M. S., Mizuta, R., Nobre, P., Satoh, M., Scoccimarro, E., Semmler, T., Small, J., and von Storch, J.-S.: High Resolution Model Intercomparison Project (HighResMIP v1.0) for CMIP6, Geosci. Model Dev., 9, 4185–4208, https://doi.org/10.5194/gmd-9-4185-2016, 2016.

Haas, R. and Pinto, J. G.: A combined statistical and dynamical approach for downscaling large-scale footprints of European windstorms, Geophys. Res. Lett., 39, L23804, https://doi.org/10.1029/2012GL054014, 2012.

Haylock, M. R.: European extra-tropical storm damage risk from a multi-model ensemble of dynamically-downscaled global climate models, Nat. Hazards Earth Syst. Sci., 11, 2847–2857, https://doi.org/10.5194/nhess-11-2847-2011, 2011.

Hersbach, H., Bell, B., Berrisford, P., Hirahara, S., Horányi, A., Muñoz-Sabater, J., Nicolas, J., Peubey, C., Radu, R., Schepers, D., Simmons, A., Soci, C., Abdalla, S., Abellan, X., Balsamo, G., Bechtold, P., Biavati, G., Bidlot, J., Bonavita, M., De Chiara, G., Dahlgren, P., Dee, D., Diamantakis, M., Dragani, R., Flem-

ming, J., Forbes, R., Fuentes, M., Geer, A., Haimberger, L., Healy, S., Hogan, R. J., Hólm, E., Janisková, M., Keeley, S., Laloyaux, P., Lopez, P., Lupu, C., Radnoti, G., de Rosnay, P., Rozum, I., Vamborg, F., Villaume, S., and Thépaut, J.-N.: The ERA5 global reanalysis, Q. J. Roy. Meteor. Soc., 146, 1999–2049, https://doi.org/10.1002/qj.3803, 2020.

Hodges, K. I.: Feature Tracking on the Unit Sphere, Mon. Weather Rev., 123, 3458–3465, https://doi.org/10.1175/1520-0493(1995)123<3458:FTOTUS>2.0.CO;2, 1995.

Hodges, K. I.: Adaptive Constraints for Feature Tracking, Mon. Weather Rev., 127, 1362–1373, https://doi.org/10.1175/1520-0493(1999)127<1362:ACFFT>2.0.CO;2, 1999.

Hodges, K. I., Lee, R. W., and Bengtsson, L.: A Comparison of Extratropical Cyclones in Recent Reanalyses ERA-Interim, NASA MERRA, NCEP CFSR, and JRA-25, J. Climate, 24, 4888–4906, https://doi.org/10.1175/2011JCLI4097.1, 2011.

Hoskins, B. J. and Hodges, K. I.: New Perspectives on the Northern Hemisphere Winter Storm Tracks, J. Atmos. Sci., 59, 1041–1061, https://doi.org/10.1175/1520-0469(2002)059<1041:NPOTNH>2.0.CO;2, 2002.

Howard, T. and Clark, P.: Correction and downscaling of NWP wind speed forecasts, Meteorol. Appl., 14, 105–116, https://doi.org/10.1002/met.12, 2007.

Hurrell, J. W. and Deser, C.: North Atlantic climate variability: The role of the North Atlantic Oscillation, J. Marine Syst., 78, 28–41, https://doi.org/10.1016/j.jmarsys.2008.11.026, 2009.

Karremann, M. K., Pinto, J. G., Reyers, M., and Klawa, M.: Return periods of losses associated with European windstorm series in a changing climate, Environ. Res. Lett., 9, 124016, https://doi.org/10.1088/1748-9326/9/12/124016, 2014.

Kennedy, J., Titchner, H., Rayner, N., and Roberts, M.: input4MIPs.MOHC.SSTsAndSeaIce.HighResMIP.MOHC-HadISST-2-2-0-0-0, version 20170505 [data set], Earth System Grid Federation, https://doi.org/10.22033/ESGF/input4MIPs.1221 (last access: 5 May 2017), 2017.

Klawa, M. and Ulbrich, U.: A model for the estimation of storm losses and the identification of severe winter storms in Germany, Nat. Hazards Earth Syst. Sci., 3, 725–732, https://doi.org/10.5194/nhess-3-725-2003, 2003.

Leckebusch, G. C., Ulbrich, U., Fröhlich, L., and Pinto, J. G.: Property loss potentials for European midlatitude storms in a changing climate, Geophys. Res. Lett., 34, L05703, https://doi.org/10.1029/2006GL027663, 2007.

Lockwood, J. F., Guentchev, G., Brown, S. J, Palin, E. J., Roberts, M. J., and Thornton, H. E.: PRIMAVERA European winter windstorm event set, Zenodo [data set], https://doi.org/10.5281/zenodo.6492182, 2022.

Mailier, P. J., Stephenson, D. B., Ferro, C. A. T., and Hodges, K. I.: Serial Clustering of Extratropical Cyclones, Mon. Weather Rev., 134, 2224–2240, https://doi.org/10.1175/MWR3160.1, 2006.

Minola, L., Zhang, F., Azorin-Molina, C., Safaei Pirooz, A. A., Flay, R. G. J., Hersbach, H., and Chen, D: Near-surface mean and gust wind speeds in ERA5 across Sweden: towards an improved gust parametrization, Clim. Dynam., 55, 887–907, https://doi.org/10.1007/s00382-020-05302-6, 2020.

Mizielinski, M. S., Roberts, M. J., Vidale, P. L., Schiemann, R., Demory, M.-E., Strachan, J., Edwards, T., Stephens, A., Lawrence, B. N., Pritchard, M., Chiu, P., Iwi, A., Churchill, J., del Cano No-

vales, C., Kettleborough, J., Roseblade, W., Selwood, P., Foster, M., Glover, M., and Malcolm, A.: High-resolution global climate modelling: the UPSCALE project, a large-simulation campaign, Geosci. Model Dev., 7, 1629–1640, https://doi.org/10.5194/gmd-7-1629-2014, 2014.

Osinski, R., Lorenz, P., Kruschke, T., Voigt, M., Ulbrich, U., Leckebusch, G. C., Faust, E., Hofherr, T., and Majewski, D.: An approach to build an event set of European windstorms based on ECMWF EPS, Nat. Hazards Earth Syst. Sci., 16, 255–268, https://doi.org/10.5194/nhess-16-255-2016, 2016.

Pinto, J. G., Bellenbaum, N., Karremann, M. K., and Della-Marta, P. M.: Serial clustering of extratropical cyclones over the North Atlantic and Europe under recent and future climate conditions, J. Geophys. Res.-Atmos., 118, 12476–12485, https://doi.org/10.1002/2013JD020564, 2013.

Pithan, F., Shepherd, T. G., Zappa, G., and Sandu, I.: Climate model biases in jet streams, blocking and storm tracks resulting from missing orographic drag, Geophys. Res. Lett., 43, 7231–7240, https://doi.org/10.1002/2016GL069551, 2016.

Prahl, B. F., Rybski, D., Burghoff, O., and Kropp, J. P.: Comparison of storm damage functions and their performance, Nat. Hazards Earth Syst. Sci., 15, 769–788, https://doi.org/10.5194/nhess-15-769-2015, 2015.

Priestley, M. D. K., Dacre, H. F., Shaffrey, L. C., Hodges, K. I., and Pinto, J. G.: The role of serial European windstorm clustering for extreme seasonal losses as determined from multi-centennial simulations of high-resolution global climate model data, Nat. Hazards Earth Syst. Sci., 18, 2991–3006, https://doi.org/10.5194/nhess-18-2991-2018, 2018.

Priestley, M. D. K., Ackerley, D., Catto, J. L., Hodges, K. I., McDonald, R. E., and Lee, R. W.: An Overview of the Extratropical Storm Tracks in CMIP6 Historical Simulations, J. Climate, 33, 6315–6343, https://doi.org/10.1175/JCLI-D-19-0928.1, 2020.

Roberts, J. F., Champion, A. J., Dawkins, L. C., Hodges, K. I., Shaffrey, L. C., Stephenson, D. B., Stringer, M. A., Thornton, H. E., and Youngman, B. D.: The XWS open access catalogue of extreme European windstorms from 1979 to 2012, Nat. Hazards Earth Syst. Sci., 14, 2487–2501, https://doi.org/10.5194/nhess-14-2487-2014, 2014.

Roberts, M. J., Baker, A., Blockley, E. W., Calvert, D., Coward, A., Hewitt, H. T., Jackson, L. C., Kuhlbrodt, T., Mathiot, P., Roberts, C. D., Schiemann, R., Seddon, J., Vannière, B., and Vidale, P. L.: Description of the resolution hierarchy of the global coupled HadGEM3-GC3.1 model as used in CMIP6 HighResMIP experiments, Geosci. Model Dev., 12, 4999–5028, https://doi.org/10.5194/gmd-12-4999-2019, 2019.

Rogers, J. C.: Patterns of Low-Frequency Monthly Sea Level Pressure Variability (1899–1986) and Associated Wave Cyclone Frequencies, J. Climate, 3, 1364–1379, https://doi.org/10.1175/1520-0442(1990)003<1364:POLFMS>2.0.CO;2, 1990.

Scaife, A. A., Arribas, A., Blockley, E., Brookshaw, A., Clark, R. T., Dunstone, N., Eade, R., Fereday, D., Folland, C. K., Gordon, M., Hermanson, L., Knight, J. R., Lea, D. J., MacLachlan, C., Maidens, A., Martin, M., Peterson, A. K., Smith, D., Vellinga, M., Wallace, E., Waters, J., and Williams, A.: Skillful long-range prediction of European and North American winters, Geophys. Res. Lett., 41, 2514–2519, https://doi.org/10.1002/2014GL059637, 2014.

Schiemann, R., Athanasiadis, P., Barriopedro, D., Doblas-Reyes, F., Lohmann, K., Roberts, M. J., Sein, D. V., Roberts, C. D., Terray, L., and Vidale, P. L.: Northern Hemisphere blocking simulation in current climate models: evaluating progress from the Climate Model Intercomparison Project Phase 5 to 6 and sensitivity to resolution, Weather Clim. Dynam., 1, 277–292, https://doi.org/10.5194/wcd-1-277-2020, 2020.

Sharkey, P., Tawn, J. A., and Brown, S. J.: A stochastic model for the lifecycle and track of extreme extratropical cyclones, arXiv [preprint], arXiv:1905.08840, 21 May 2019, 2019.

Sharkey, P., Tawn, J. A., and Brown, S. J.: Modelling the spatial extent and severity of extreme European windstorms, J. R. Stat. Soc. C, 69, 223–250, https://doi.org/10.1111/rssc.12391, 2020.

Small, R. J., Msadek, R., Kwon, Y.-O., Booth, J. F., and Zarzycki, C.: Atmosphere surface storm track response to resolved ocean mesoscale in two sets of global climate model experiments, Clim. Dynam., 52, 2067–2089, https://doi.org/10.1007/s00382-018-4237-9, 2019.

Smith, D. M., Scaife, A. A., Eade, R., Athanasiadis, P., Bellucci, A., Bethke, I., Bilbao, R., Borchert, L. F., Caron, L.-P., Counillon, F., Danabasoglu, G., Delworth, T., Doblas-Reyes, F. J., Dunstone, N. J., Estella-Perez, V., Flavoni, S., Hermanson, L., Keenlyside, N., Kharin, V., Kimoto, M., Merryfield, W. J., Mignot, J., Mochizuki, T., Modali, K., Monerie, P.-A., Müller, W. A., Nicolí, D., Ortega, P., Pankatz, K., Pohlmann, H., Robson, J., Ruggieri, P., Sospedra-Alfonso, R., Swingedouw, D., Wang, Y., Wild, S., Yeager, S., Yang, X., and Zhang, L.: North Atlantic climate far more predictable than models imply, Nature, 583, 796–800, https://doi.org/10.1038/s41586-020-2525-0, 2020.

Solvency II: Directive 2009/138/EC of the European Parliament and of the Council of 25 November 2009 on the taking-up and pursuit of the business of Insurance and Reinsurance (Solvency II) (Text with EEA relevance) OJ L 335, 17.12.2009, 1–155, http://data.europa.eu/eli/dir/2009/138/oj (last access: November 2021), 2009.

Steptoe, H.: C3S WISC Event Set Description, technical report, https://web.archive.org/web/20220127184701/https://wisc.climate.copernicus.eu/wisc/documents/shared/C3S_WISC_EventSet_Description_v1.0.pdf (last access: November 2022), 2017.

Swiss Re: Sigma No 1/2018: Natural catastrophes and man-made disasters in 2017: a year of record-breaking losses, https://www.swissre.com/dam/jcr:1b3e94c3-ac4e-4585-aa6f-4d482d8f46cc/sigma1_2018_en.pdf (last access: November 2022), 2018.

Tamarin-Brodsky, T. and Kaspi, Y.: Enhanced poleward propagation of storms under climate change, Nat. Geosci., 10, 908–913, https://doi.org/10.1038/s41561-017-0001-8, 2017.

Vitolo, R., Stephenson, D. B., Cook, I. M., and Mitchell-Wallace, K: Serial clustering of intense European storms, Meteorol. Z., 18, 411–424, https://doi.org/10.1127/0941-2948/2009/0393, 2009.

Voldoire, A., Saint-Martin, D., Sénési, S., Decharme, B., Alias, A., Chevallier, M., Colin, J., Guérémy, J.-F., Michou, M., Moine, M.-P., Nabat, P., Roehrig, R., Salas y Mélia, D., Séférian, R., Valcke, S., Beau, I., Belamari, S., Berthet, S., Cassou, C., Cattiaux, J., Deshayes, J., Douville, H., Franchisteguy, L., Ethé, C., Geoffroy, O., Lévy, C., Madec, G., Meurdesoif, Y., Msadek, R., Ribes, A., Sanchez-Gomez, E., Terray, L.: Evaluation of CMIP6 DECK

https://doi.org/10.5194/nhess-22-3585-2022

Nat. Hazards Earth Syst. Sci., 22, 3585–3606, 2022

Experiments with CNRM-CM6-1, J. Adv. Model. Earth Sy., 11, 2177–2213, https://doi.org/10.1029/2019MS001683, 2019.

Wallace, J. M. and Gutzler, D. S.: Teleconnections in the Geopotential Height Field during the Northern Hemisphere Winter, Mon. Weather Rev., 109, 784–812, https://doi.org/10.1175/1520-0493(1981)109<0784:TITGHF>2.0.CO;2, 1981.

Walz, M. A. and Leckebusch, G. C.: Loss potentials based on an ensemble forecast: How likely are winter windstorm losses similar to 1990?, Atmos Sci Lett., 20, e891, https://doi.org/10.1002/asl.891, 2019.

Welker, C., Röösli, T., and Bresch, D. N.: Comparing an insurer's perspective on building damages with modelled damages from pan-European winter windstorm event sets: a case study from Zurich, Switzerland, Nat. Hazards Earth Syst. Sci., 21, 279–299, https://doi.org/10.5194/nhess-21-279-2021, 2021.

Williams, K. D., Copsey, D., Blockley, E. W., Bodas-Salcedo, A., Calvert, D., Comer, R., Davis, P., Graham, T., Hewitt, H. T., Hill, R., Hyder, P., Ineson, S., Johns, T. C., Keen, A. B., Lee, R. W., Megann, A., Milton, S. F., Rae, J. G. L., Roberts, M. J., Scaife, A. A., Schiemann, R., Storkey, D., Thorpe, L., Watterson, I. G., Walters, D. N., West, A., Wood, R. A., Woollings, T., and Xavier, P. K.: The Met Office Global Coupled model 3.0 and 3.1 (GC3.0 & GC3.1) configurations, J. Atmos. Model. Earth Sy., 10, 357–380, https://doi.org/10.1002/2017MS001115, 2018.

Williams, K. D., van Niekerk, A., Best, M. J., Lock, A. P., Brooke, J. K., Carvalho, M. J., Derbyshire, S. H., Dunstan, T. D., Rumbold, H. S., Sandu, I., and Sexton, D. M. H.: Addressing the causes of large-scale circulation error in the Met Office Unified Model, Q. J. Roy. Meteor. Soc., 146, 2597–2613, https://doi.org/10.1002/qj.3807, 2020.

Willison, J., Robinson, W. A., and Lackmann, G. M.: The Importance of Resolving Mesoscale Latent Heating in the North Atlantic Storm Track, J.Atmos. Sci., 70, 2234–2250, https://doi.org/10.1175/JAS-D-12-0226.1, 2013.

Wood, N. and Mason, P.: The pressure force induced by neutral, turbulent flow over hills, Q. J. Roy. Meteor. Soc., 119, 1233–1267, https://doi.org/10.1002/qj.49711951402, 1993.

World Meteorological Organization (WMO): Measurement of surface wind, in: Guide to Instruments and Methods of Observation Volume I – Measurement of Meteorological Variables, 2018 edition, World Meteorological Organization, Geneva, Switzerland, https://library.wmo.int/doc_num.php?explnum_id=10616 (last access: 4 January 2022), 2018.

Youngman, B. D. and Stephenson, D. B.: A geostatistical extreme-value framework for fast simulation of natural hazard events, P. R. Soc. A, 472, 2189, https://doi.org/10.1098/rspa.2015.0855, 2016.

Zappa, G., Shaffrey, L. C., and Hodges, K. I.: The ability of CMIP5 models to simulate North Atlantic extratropical cyclones, J. Climate, 26, 5379–5396, https://doi.org/10.1175/JCLI-D-12-00501.1, 2013.